Karlsruhe Institute of Technology

**Elektrotechnisches Institut (ETI)**
Prof. Dr.-Ing. Michael Braun
Prof. Dr.-Ing. Martin Doppelbauer
Prof. Dr.-Ing. Marc Hiller
Kaiserstr.12. 76131 Karlsruhe

Elektrotechnisches Institut

| | |
|---|---|
| Title: | Investigations on the Experimental Identification of AC-Copper Losses in Permanent Magnet Synchronous Machines using a Motor Sub-Assembly |
| Authors: | Christoph Rollbühler, Sebastian Peukert, Daniel Fritz, Jean-Francois Heyd, Johannes Kolb, Martin Doppelbauer |
| Institute: | Karlsruhe Institute of Technology (KIT)<br>Institute of Electrical Engineering (ETI)<br>Hybrid Electric Vehicles (HEV) |
| Type: | Conference Proceedings |
| Published at: | Proceedings IECON 2019 - 45th Annual Conference of the IEEE Industrial Electronics Society<br>Publisher: IEEE<br>Year: 2019<br>ISBN: 978-1-7281-4878-6<br>Pages: 1150-1156 |
| Hyperlinks: | https://ieeexplore.ieee.org/document/8926835 |

# Investigations on the Experimental Identification of AC-Copper Losses in Permanent Magnet Synchronous Machines using a Motor Sub-Assembly

Christoph Rollbühler
*Institute of Electrical Engineering*
*Karlsruhe Institute of Technology*
Karlsruhe, Germany
c.rollbuehler@kit.edu

Sebastian Peukert
*Institute of Electrical Engineering*
*Karlsruhe Institute of Technology*
Karlsruhe, Germany

Daniel Fritz
*Institute of Electrical Engineering*
*Karlsruhe Institute of Technology*
Karlsruhe, Germany

Jean-Francois Heyd
*Schaeffler Automotive Buehl*
*GmbH&Co.KG*
Bühl, Germany

Johannes Kolb
*SHARE at KIT*
*Schaeffler Technologies AG & Co. KG*
Karlsruhe, Germany

Martin Doppelbauer
*Institute of Electrical Engineering*
*Karlsruhe Institute of Technology*
Karlsruhe, Germany

***Abstract*—Analysis of AC copper losses in electrical machines is still a challenging task. Due to high utilization of high power density automotive drives, stray fields in the slots cause a significant copper loss increase compared to DC copper losses. Especially at large cross-sectional areas of the wires up to several times the DC-losses may occur in copper. This paper presents a new method of identifying these additional copper losses in electrical machines directly through measurement and without any finite-element co-simulation, which has not been shown in literature so far. Therefore, a motor sub-assembly consisting of three stator-teeth of an automotive machine and a rotor back iron are manufactured. Different adaptations of the motor sub-assembly are analysed using finite-element software to ensure proper flux-paths and AC copper losses close to the motor. Finally, measurements are performed and discussed.**

***Keywords — current displacement, proximity loss, copper loss, interior permanent magnet synchronous machine, motorette***

## I. Introduction

For proper electrical machine design, knowledge about losses and their origin is important. Especially in the case of highly utilized permanent magnet synchronous machines for electric traction drives, good efficiency is needed to allow a large driving range. Hence, losses have to be known and minimized. The main losses in electrical machines are produced in the copper windings and the stator iron.

Iron losses are a well-studied topic, with a large amount of publications focusing on the modelling of the losses of single iron sheets [1–10]. Furthermore, there are standardized testbenches such as Epstein frames [11] and Single Sheet Testers [12]. These make it possible to analyse a wide range of measurement data. Ongoing studies focus on measuring and evaluating the influences of production processes like different separation and joining processes to get more accurate models of the core losses [13–18]. Copper losses on the other hand are mainly evaluated using the DC value of the winding resistance, which is not accurate. Copper-losses caused by current displacement effects (CDE) in the windings of electrical machines can increase up to several times the losses modelled with the DC value of the stator resistance [3, 19–21]. Current displacement is caused by skin and proximity effect. The high magnetic utilization in traction application results in saturation of the stator iron even at low current levels. This causes a great amount of stray-flux in the slots and thus leads to a further increase of the proximity effect. In literature, most authors focus on analysing AC copper losses using finite-element (FE) software. FE-calculations provide good results – in contrast to calculation of iron losses. However, by using FE-software production-based influences such as the exact position of the windings, as well as generation of thermal hot spots, cannot be evaluated. Moreover, most FE analyses are based on two-dimensional calculations and therefore cannot represent end-winding effects. This is why motor sub-assemblies (or so-called motorettes) are used to analyse and measure AC winding losses.

In literature, arrangements of three stator-teeth are already presented in [19, 22, 23]. However, only one of the three teeth is wound with copper wire. For this reason, only symmetric flux-paths can be caused in the arrangement. [24] and [25] show that asymmetric flux-paths in the stator-teeth are also possible, especially under load-condition. Furthermore, there is no substitute for the rotor of an electric machine, like e.g. a rotor back iron, in the arrangement. To ensure flux paths, which are close to the flux in the real machine, this is mandatory.

On that account, a new experimental approach to evaluate AC winding losses, based on past work [19, 22, 23], is presented in this paper. To improve the characteristics, a rotor back iron and three instead of one winding are used. Furthermore, the proposed approach determines additional copper losses directly by measurement. The experiment is performed to confirm the great amount of current displacement losses in simulation.

Modelling of the new testbench is discussed in section II. FE-simulations of the sub-assembly show a good accordance of the flux paths compared to the machine, thus providing the proof of the concept. An equivalent circuit diagram is proposed. Section III gives a short overview of the new testbench, the used measurement equipment and power electronics. In section IV and V, the measurement principle is proposed and results are presented. The conclusion of the paper is given in section VI.

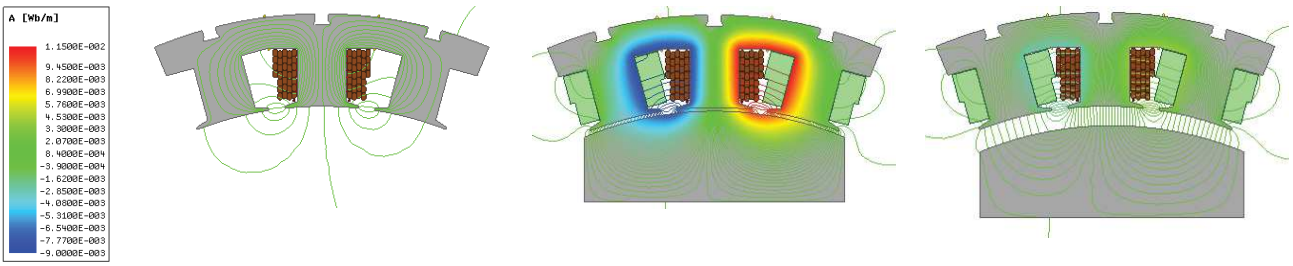


(a) MTT,ST (b) MTT (c) MTT,AG

Fig. 1: flux lines of the different motorette setups excited with 20 A peak winding current each

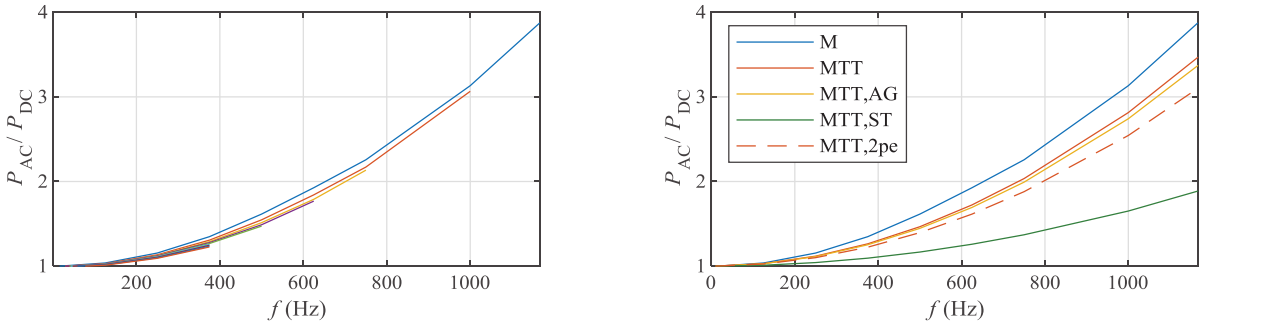


(a) copper loss ratio of the motor for different torque reference values

(b) copper loss ratio of the motor and different motorette setups for 16 A peak winding current.

Fig. 2: comparison of the $P_{AC}/P_{DC}$ loss ratio of the motor and the three motorette modifications for different operating points

## II. Modelling of the Proposed Setup

Current displacement in electric machines is caused by skin and proximity effect, especially if there is an intense stray field in the slots. Due to high utilization of the stator iron, parts of the stator teeth saturate even at low current levels and cause stray flux in the slots. This stray flux induces voltage in the windings and causes current displacement, which is attributed to the proximity effect. In comparison to the current displacement caused by stray flux, the impact of the pure skin effect in automotive traction drives is very low. For example, the skin depth for a round wire with the same cross sectional area as the given motors winding at maximum speed is 2.04mm, which is greater than the diameter of this equivalent copper wire.

In this publication, three different motorette setups, shown in Fig. 1 (a) to (c), are modelled numerically and analytically. First, the motorette setups are analysed using Ansys Maxwell FE-software to ensure proper flux paths and to compare the setups to the actual machine's electromagnetic behaviour. An important target for measuring comparable operating points is to have the same magnetic flux in the motorette as in the real motor application. The modelling of the setup of interest, MTT, is performed in section A. The modifications of this arrangement are analysed and compared to MTT in section B, in section C the analytic model of the testbench is defined.

### *A. Numerical Modelling*

The geometry shown in Fig. 1 (b), as well as the complete motor geometry are simulated. At first, losses of the motor winding operated with maximum torque per ampere (MTPA) currents are analysed. Therefore, the AC copper loss to DC copper loss ratio $P_{AC}/P_{DC}$ is used. $P_{DC}$ denotes the loss in copper without any current displacement effects, so it can be simply calculated via stranded conductors or with ( 1 ) :

$$P_{DC} = R(\vartheta) \cdot \frac{1}{T} \int_0^T i^2(t)\, \mathrm{d}t \qquad (1)$$

$R$ equals the full winding resistance, thus containing the end-winding. This has to be considered when calculating the simulated CDE-losses as the FE simulation is performed in 2D and an end-winding is not part of the model. $P_{AC}$ though describes all losses occurring in copper, so the DC-part ($P_{DC}$) as well as the additional losses due to current displacement effects $P_{CDE}$:

$$P_{AC} = P_{DC} + P_{CDE}. \qquad (2)$$

To ensure proper simulation results, each observed conductor is modelled solid, see Fig. 4 (a). CDE effects in the end-windings are neglected, because the winding head of the investigated machine is small. By building the ratio the additional CDE-losses can be quantified and corresponded to the DC loss part.

The $P_{AC}/P_{DC}$ characteristic of the motor in Fig. 2 (a) shows little dependency on the torque reference values, but a quadratic dependency on the excitation frequency. This characteristic is compared to different motorette setups in Fig. 2 (b).

The motorette setup is analysed using the same current amplitude as in the motor simulation. In Fig. 2 (b) the copper loss ratio of the motor (M, —) and the motorette (MTT, —) for a current corresponding to a quarter of maximum torque is shown. The figure shows a good accordance of the additional copper-losses in the motor and the motorette over speed. For small frequencies, $P_{AC}/P_{DC}$ is nearly the same, but with increasing electrical frequency, losses in the motorette under-

estimate the losses in the motor. The motorette has a $P_{AC}/P_{DC}$-ratio of 3.5 at maximum frequency, whereby the motor has an $P_{AC}/P_{DC}$ -ratio of 3.9. Thus, the motorette losses would underestimate the real CDE-losses in the motor around 10%. The deviations have to be clarified to ensure a motorette-behaviour close to the real machine. Main difference to the motor are the missing permanent magnets. Since placing magnets in the motorette is not expedient, as the high flux has to be compensated by the windings and only one rotor angle of the machine can be modelled, a possible approximation is considering the permeability of the magnets by an extra air gap increase. This is investigated in Section B, as well as the modification of the motorette in Fig. 1 (a).

### *B. Modifications of the Setup*

To get a detailed knowledge of the testbench design parameters, different modifications of the proposed setup are analysed in FE-simulation. Two of them are compared to the proposed setup MTT in this section. On the one hand, a three-tooth arrangement with only one winding is simulated to justify the usage of three windings: MTT,ST. On the other hand the influence of the machines permanent magnets on the magnetic circuit is examined using a three-tooth-arrangement with a bigger air gap: $\delta_{MTT,AG} = \delta_{motor} + h_{PM}$. Here, $h_{PM}$ equals the height of the machines permanent magnets. This yields to the results of MTT,AG. The three arrangements as well as the occurring flux lines are shown in Fig. 1.

MTT,ST is a typical implementation of a motorette for thermal modelling and material testing. It is used in [19, 22, 23] for example. The magnetic resistance of the arrangement is high due to the large air gap, so the flux in tooth B is low. In addition, the stray flux in the slots does not represent the conditions in a real motor application. This lack of high flux densities in tooth B, as well as the "false" stray flux in the slots, is improved by arrangement b), the proposed motorette MTT. An additional rotor back iron reduces the magnetic resistance of the magnetic circuit and therefore allows for higher flux densities in tooth B at the same current excitation. Furthermore, the stray flux in the slots is near to the one in a real motor application. Fig. 2 (b) shows clearly that the behaviour of MTT (—) is closer to the motor (—) than the behaviour of MTT,ST (—). Especially at higher frequencies, MTT,ST shows larger deviations to the motor.

MTT shows a comparable characteristic as the motor itself, but underestimates the losses for every given operating point. A possible reason are the motors permanent magnets. It is not expedient to insert magnets in the arrangement, because they cause a constant flux-offset instead of a rotating flux. Furthermore, [27] shows that the influence of the magnets on current displacement losses is low. As permanent magnets have a permeability close to air, the magnetic resistance of the magnetic circuit is increased by $R_{m,PM} \approx h_{PM}/(\mu_0 * A_{PM})$ due to the permanent magnets. This also can be achieved by adding an additional air gap in arrangement c): MTT,AG. As a result, the AC copper loss ratio of MTT,AG is given in Fig. 2 (b, —). However $P_{AC}/P_{DC}$ stays below the initial approach MTT, therefore this modification is not reasonable. A further drawback of the large air gap is a very high voltage demand.

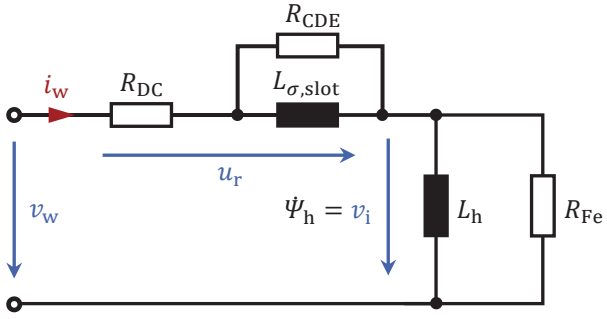


Fig. 3: equivalent circuit diagram of one winding of the presented motorette

Summing up, MTT shows a behaviour that is closer to the motor than the other modifications. Flux lines as well as the $P_{AC}/P_{DC}$-ratio are close to the real machine. For this reason measurements are performed using the MTT setup, see section V.

### *C. Equivalent Circuit Diagram*

In Fig. 3 the equivalent circuit diagram of one winding of the motorette is presented. $v_w$ represents the feeding voltage, $v_i$ the induced voltage in the considered winding. $R_{Fe}$ denotes the iron loss resistance of the model, $R_{DC}$ describes the losses due to the ohmic part of the circuit and $R_{CDE}$ the losses due to current displacement effects. As the current displacement effects are primary dependent on the stray field of the slots, $R_{CDE}$ is located in parallel to the stray-field inductance of the phase.

## III. Experimental Motorette Setup

To measure additional AC copper losses, three single teeth of an electrical machine are joined to a so-called motorette: First, the individual teeth are wound with copper wire. Then the three teeth are mechanically pressed together to form a triple bond. An additional rotor back iron is used to ensure proper flux paths in the motorette. The air-gap distance is defined using a suitable sheet of silicon. Fig. 4 (a) shows the cross-sectional view of the motorette. Due to the three teeth and the rotor back iron, the magnetic circuit for the central tooth is close to the real motor. Therefore, the flux conditions of the central tooth are close to the real application and the behaviour of current displacement is comparable to motor application. All iron parts are manufactured using NO20 sheets.

The resulting air gap $\delta_{MTT}$ between the stator tooth arrangement and the rotor back iron is derived from the original motor. The motor of interest is an interior permanent magnet synchronous machine with 170 Nm nominal torque and a maximum speed of 7000 rpm. Due to the high number of poles (20), the electric frequency during application can reach 1167 Hz. Profile-Windings with a cross-sectional area of 2.78 mm² are used as concentrated single-tooth winding without parallel strands.

Fig. 4 (b) shows the simplified schematic of the testbench. Each winding of the motorette is supplied by a H-bridge converter, using IGBT-modules of type *Infineon FS75R12KT4_B15*. The converters share a common DC-Link with an adjustable voltage and have a switching frequency of 15 kHz. Signal processing and control is managed by a self-developed digital signal processing system [26]. Gate signals

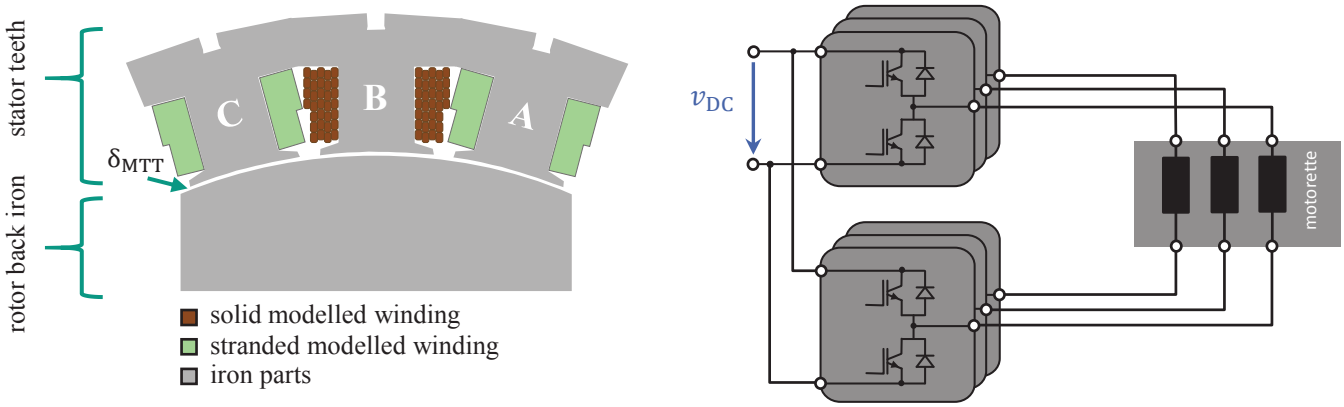


(a) cross-sectional view of the motorette

(b) simplified schematic of the testbench

Fig. 4: motorette cross-sectional view and testbench overview

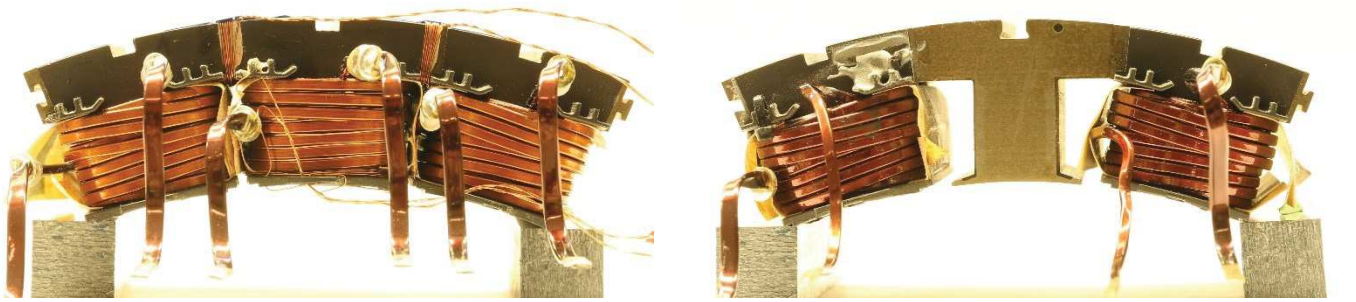

Fig. 5: winding arrangement of the two motorette variations. Left side: variation I, Right side: variation II. Thin copper wires are used as auxiliary flux measuring windings in the yoke and near the airgap during commissioning.

are created by a modulator using unipolar switching. The resulting switching frequent current ripple is negligibly small. Measured quantities for power analysis in the measurement section are acquired using a *LeCroy WaveRunner HRO 64Zi* oscilloscope with *Tektronix P5200A* voltage and *Tektronix A6303* current probes.

Referring to section IV two variations of the motorette setup, which are presented in Fig. 5, are needed. Both are based on the same three-tooth-arrangement. At the second variation, the centre winding is removed. Furthermore, an auxiliary measurement winding wound around the tooth in the centre is visible. It is used to measure the flux linkage by means of the induced voltage of the tooth.

## IV. Measurement Principle

Current displacement losses are determined via a two-step analysis. Therefore two motorettes are built and measured: One motorette with three windings (variation I), and one motorette with only two, missing the centre winding B (variation II), see Fig. 5. Excitation is performed at the both outer windings, the principle is explained in detail in section A. The provided power for both arrangements is subtracted from each other. The difference forms the current displacement losses in the middle winding of variation I. The calculation is shown in section B.

Measurements are performed at the same winding temperature to ensure comparable boundary conditions. In [28] a method of scaling the current displacement loss with temperature is proposed. So the measured loss of the motorette at a given temperature can be projected to motor operation.

### A. Excitation

Under three phase excitation (3pe) the three stator teeth are exposed to a certain alternating current, e.g. derived from MTPA values of the existing motor. Hence, the winding arrangement has to be the same as in the motor, e.g. for teeth A to C: U-V-W or U-V-V, depending on the coil grouping of the machine. As only the two outer windings are used to excite the two variations of the motorette, a special method of excitation, which is called two phase excitation (2pe) in the following, is needed.

The magnetic circuit of the motorette is modelled in Fig. 6 and the flux in tooth B results from the following equation:

$$\Phi_{\mathrm{B}} = \frac{\theta_{\mathrm{A}} - 2\theta_{\mathrm{B}} + \theta_{\mathrm{C}}}{K\left(-1 - 2\frac{R_{\mathrm{m,Z}} + R_{\mathrm{m},\delta}}{K}\right)}, \quad (3)$$

$$\mathrm{K} = R_{\mathrm{m,Z}} + R_{\mathrm{m,J}} + R_{\mathrm{m},\delta} + R_{\mathrm{m,R}} \quad (4)$$

The current of tooth B is added to the outer teeth in a way that the same flux in tooth B is present:

- *Three phase excitation:* the teeth A to C are supplied with $i_{\mathrm{A,3pe}}(t), i_{\mathrm{B,3pe}}(t)$ and $i_{\mathrm{C,3pe}}(t)$ resulting in the corresponding flux values $\Phi_{\mathrm{A,3pe}}(t), \Phi_{\mathrm{B,3pe}}(t), \Phi_{\mathrm{C,3pe}}(t)$.
- *Two phase excitation:* To ensure the same flux as in three phase excitation ( $\Phi_{\mathrm{B,2pe}} := \Phi_{\mathrm{B,3pe}}$ ), $i_{\mathrm{B,3pe}}(t)$ is subtracted from Winding A, B and C in the way, that:

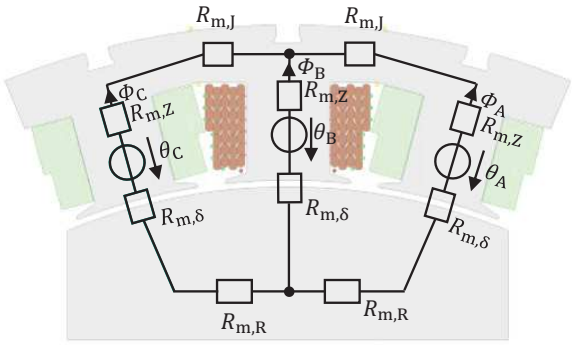


Fig. 6: magnetic circuit of the proposed motorette

- $i_{A,2pe}(t) = i_{A,3pe}(t) - i_{B,3pe}(t)$
- $i_{B,2pe}(t) = i_{B,3pe}(t) - i_{B,3pe}(t) = 0$
- $i_{C,2pe}(t) = i_{C,3pe}(t) - i_{B,3pe}(t)$

resulting in

- $\theta_{A,2pe}(t) = \theta_{A,3pe}(t) - \theta_{B,3pe}(t)$
- $\theta_{B,2pe}(t) = \theta_{B,3pe}(t) - \theta_{B,3pe}(t) = 0$
- $\theta_{C,2pe}(t) = \theta_{C,3pe}(t) - \theta_{B,3pe}(t)$.

This yields the same numerator in ( 3 ), resulting in the same flux in tooth B as in three phase excitation.

Fig. 7 shows the resulting currents in three and two phase excitation as well as the induced voltages in the auxiliary winding of tooth B. For this purpose motorette variation I is used. To ensure no influences of the converter in two phase excitation, the terminals of tooth B are disconnected. The resulting induced voltages of the auxiliary measurement winding of tooth B are nearly the same, which means that the flux relations are comparable. This proves the assumption of a magnetically equal operating point.

Summing up, in two phase excitation, nearly the same flux as in three phase excitation is applied to the motorette: $\Phi_{B,2pe} \approx \Phi_{B,3pe}$, so the winding is exposed to nearly the same magnetic field. This means that the testbench is in the same magnetic operating condition as if three windings are supplied with current, and therefore comparison to motor operation is possible. In Fig. 2 (b) the estimated copper loss ratio of two phase excitation is plotted as dashed red line (– –).

The currents of the testbench are controlled by means of a repetitive current controller, to ensure a good sinusoidal waveform. Application of a PI controller for alternating currents is not sufficient, as it leads to errors in phase or amplitude.

The controller is calculating the difference of the measured current $i_i$ and the reference current $i_i^*$ in every switching cycle. This difference is stored in a look up table with its associated electric angle. The stored data is used as error memory and fed forward in the next electrical period $i + 1$ at the associated electric angle $\gamma$. A damping factor k, k ∈ [0,1], is used to soften high frequent disturbances:

$$err_{i+1}(\gamma) = k \cdot \left(i_i^*(\gamma) - i_i(\gamma)\right) + err_i(\gamma) \qquad (5)$$

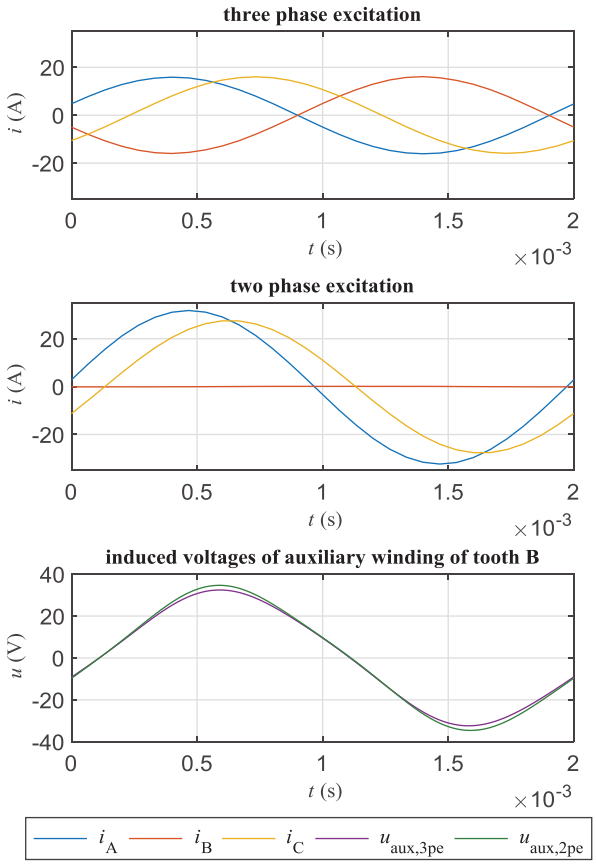


Fig. 7: measured currents and voltages of three and two phase excitation of the motorette for 16 A peak winding current and 500 Hz excitation frequency

The error is reduced iteratively, as displayed in Fig. 8. Here, the absolute value of the error for every angle is integrated over a whole electrical period $T_e$, leading to a value which quantifies the quality of the actual current waveform. Once the value of the integral falls below 5% of the area of the reference signal, the control process is terminated and the measurement is performed. Thus comparable control results are generated and the signal quality is guaranteed.

## *B. Loss Calculation*

Loss calculation is performed by comparing the applied power of the two motorette variations. Since variation II has no winding around tooth B in the centre, no losses due to current displacement in this winding are possible. However, the winding around the centre tooth of variation I causes current displacement losses. Due to the fact, that the currents exciting motorette variation I and II are the same, they lead to the same flux characteristics for the testbench. Therefore, all other losses stay constant. A simple subtraction of the losses of both variations results in the additional current displacement losses of the motorette:

$$P_{CDE} = P_{\text{variation I}} - P_{\text{variation II}} \qquad (6)$$

$$P_{\text{variation}} = P_{\text{in}} - P_{\text{out}} = \text{mean}\left(u_A(t) \cdot i_A(t) - u_C(t) \cdot i_C(t)\right) \qquad (7)$$

DC losses are obtained by ( 1 ), using the current of three phase excitation because the occurring CDE-losses are referred to this current value.

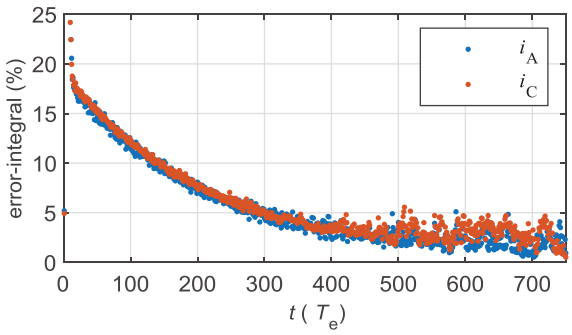


Fig. 8: step response of controllers error integral

## V. Measurement Results

Measurements in Fig. 9 show a significant increase in current displacement losses over frequency (—). Six series of measurements are performed with an excitation current amplitude $\hat{\imath}_A$ and $\hat{\imath}_C$ of 20 A and frequencies equal to 125, 500 and 1000 Hz. The measured CDE-loss rises up to 14.92 W in average at 1000 Hz. The estimated quadratic behaviour of $P_{CDE}$ is visible. The black error bars show the standard deviation of the six measurements, which are between 1 W and 2.5 W.

Comparing the AC losses to the equivalent DC loss in copper results in the red curve of Fig. 9, denoted as $P_{AC}/P_{DC}$. A multiplication of 2.3 times is measured. Compared to the simulations (– –) the measured loss ratio fits good over the frequency range.

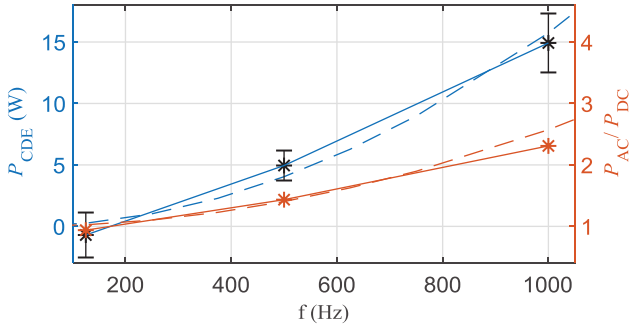


Fig. 9: measured additional loss $P_{CDE}$ due to current displacement and $P_{AC}/P_{DC}$-loss ratio for 20 A peak winding current. Measured frequencies are marked with a *, the dashed line represents the simulated values for $P_{AC}/P_{DC}$.

## VI. Conclusions and Future Work

This paper presents a new experimental approach to evaluate AC winding losses in a motor sub-assembly. The integration of a rotor back iron makes it possible to ensure motor-like flux paths in the slot. AC winding losses are determined directly through measurement, no FE co-simulation separating iron-loses is needed. Hence, the new approach offers an economic and easy method of determining AC winding losses since only a part of the stator is needed.

First measurements show a significant increase of the losses over frequency due to current displacement and a good accordance to simulation. Furthermore, the additional CDE loss compared to the ohmic DC loss is remarkable. The confirmation of the simulated current displacement losses shows the significance of a better model for electric machines to cope with the influences of current displacement on the overall machine loss. A first model is introduced in Fig. 3. Simple models, which only include the ohmic resistance measured in DC-excitation, falsify the power balance of an electric machine. Either they underestimate the real losses in copper or the missing loss shares are assigned to the iron. In FE analysis, an adaption to solid modelled coils is sufficient, but time-consuming. Based on the results of this publication this additional effort of investigating current displacement effects is necessary.

The confirmation of the simulated current displacement losses also shows that the numerical calculation of CDE losses yields reliable results. On that account influences due to manufacturing like exact positioning of the windings, thermal hotspots as well as end-winding effects can be covered by FE-simulations correctly.

In the future, we aim to perform additional measurements. For example, other winding arrangements can be tested. Especially windings with big cross-sectional areas open an interesting field of testing, e.g. hairpin-windings. In addition, analysis of windings with parallel strands is possible.

## VII. References


[1] G. Bertotti, “General properties of power losses in soft ferromagnetic materials,” *IEEE Trans. Magn.*, vol. 24, no. 1, pp. 621–630, 1988.

[2] G. Bertotti, *Hysteresis in magnetism: For physicists, materials scientists and engineers*. San Diego, Calif.: Acad. Press, 1998.

[3] C. Carstensen, *Eddy Currents in Windings of Switched Reluctance Machines*. Dissertation. Aachen: Shaker, 2007.

[4] L. R. Dupre and J. Melkebeek, “Electromagnetic hysteresis modelling: from material science to finite element analysis of devices,” *International Compumag Society Newsletter*, vol. 2003, pp. 4–15, 2003.

[5] D. Eggers, S. Steentjes, and K. Hameyer, “Advanced Iron-Loss Estimation for Nonlinear Material Behavior,” *IEEE Trans. Magn.*, vol. 48, no. 11, pp. 3021–3024, 2012.

[6] F. Preisach, “Über die magnetische Nachwirkung,” 1935.

[7] J. Gyselinck *et al.*, “Calculation of eddy currents and associated losses in electrical steel laminations,” *IEEE Trans. Magn.*, vol. 35, no. 3, pp. 1191–1194, 1999.

[8] E. Hristoforou, Ed., *SMM 2011: 20th international conference on Soft magnetic materials, 18-22 September 2011, Kos Island, Greece : abstracts book and conference program*. Piraeus: X. Mpenou, op. 2011.

[9] I. D. Mayergoyz, *Mathematical Models of Hysteresis and their Applications,* 2nd ed. Burlington: Elsevier, 2003.

[10] D. Schmidt, F. Henrotte, and K. Hameyer, “Improved iron loss prediction by a modified Bertotti-loss-

equation," in *SMM 2011: 20th international conference on Soft magnetic materials, 18-22 September 2011, Kos Island, Greece : abstracts book and conference program*, E. Hristoforou, Ed., Piraeus: X. Mpenou, op. 2011.

[11] *Magnetische Werkstoffe – Teil 2: Verfahren zur Bestimmung der magnetischen Eigenschaften von Elektroband und -blech mit Hilfe eines Epsteinrahmens*, 60404-2, 2009.

[12] Forschungsvereinigung Antriebstechnik e.V., Ed., *Weichmagnetische Werkstoffe: Aufbau einer Materialdatenbank unterschiedlicher Elektrobandgüten für den Einsatz in Kfz-Elektromotoren*: Forschungsvereinigung Antriebstechnik e.V., 2015.

[13] M. Hofmann, H. Naumoski, U. Herr, and H.-G. Herzog, "Magnetic Properties of Electrical Steel Sheets in Respect of Cutting: Micromagnetic Analysis and Macromagnetic Modeling," *IEEE Trans. Magn.*, vol. 52, no. 2, pp. 1–14, 2016.

[14] E. Lamprecht, M. Homme, and T. Albrecht, "Investigations of eddy current losses in laminated cores due to the impact of various stacking processes," in *2012 2nd International Electric Drives Production Conference (EDPC)*, pp. 1–8.

[15] M. Veigel and M. Doppelbauer, "Analytic modelling of magnetic losses in laminated stator cores with consideration of interlamination eddy currents," in *2016 XXII International Conference on Electrical Machines (ICEM)*, pp. 1339–1344.

[16] M. Veigel, A. Kramer, G. Lanza, and M. Doppelbauer, "Investigation of the impact of production processes on iron losses of laminated stator cores for electric machines," in *2016 IEEE Energy Conversion Congress and Exposition (ECCE)*, pp. 1–5.

[17] M. Veigel, P. Winzer, J. Richter, and M. Doppelbauer, "New FPGA-based and inline-capable measuring method for the identification of magnetic losses in electrical steel," in *Proceedings of International Electric Drives Production Conference (EDPC)*, Nuremberg, Germany, 2015, pp. 1–6.

[18] A. Schoppa, J. Schneider, C.-D. Wuppermann, and T. Bakon, "Influence of welding and sticking of laminations on the magnetic properties of non-oriented electrical steels," *Journal of Magnetism and Magnetic Materials*, vol. 254-255, pp. 367–369, 2003.

[19] Phil Mellor, Rafal Wrobel, Daniel Salt, Antonio Griffo, "Experimental and Analytical Determination of Proximity Losses in a High-Speed PM Machine," in *15-19 Sept. 2013, Colorado Convention Center, Denver, CO*.

[20] D. Bauer, P. Mamuschkin, H.-C. Reuss, and E. Nolle, "Influence Of Parallel Wire Placement On The AC Copper Losses In Electrical Machines,"

[21] S. Iwasaki *et al.,* "Influence of PWM on the Proximity Loss in Permanent-Magnet Brushless AC Machines," in *2015 IEEE International Electric Machines & Drives Conference (IEMDC)*, pp. 1359–1367.

[22] R. Wrobel, D. E. Salt, A. Griffo, N. Simpson, and P. H. Mellor, "Derivation and Scaling of AC Copper Loss in Thermal Modeling of Electrical Machines," *IEEE Trans. Ind. Electron.*, vol. 61, no. 8, pp. 4412–4420, 2014.

[23] P. Mellor, R. Wrobel, and N. McNeill, "Investigation of Proximity Losses in a High Speed Brushless Permanent Magnet Motor," in *Conference Record of the 2006 IEEE Industry Applications Conference Forty-First IAS Annual Meeting*, pp. 1514–1518.

[24] L. Ma, M. Sanada, S. Morimoto, and Y. Takeda, "Iron loss prediction considering the rotational field and flux density harmonics in IPMSM and SynRM," *IEE Proc., Electr. Power Appl.*, vol. 150, no. 6, p. 747, 2003.

[25] Marc Veigel, *Neues Messverfahren zur Bestimmung der fertigungsabhängigen Eisenverluste von Stator-Einzelzahnblechpaketen in Synchronmaschinen*. Dissertation. Karlsruhe: KIT, 2018.

[26] C. Axtmann, M. Boxriker, and M. Braun, "A custom, high-performance real time measurement and control system for arbitrary power electronic systems in academic research and education," in *2016 18th European Conference on Power Electronics and Applications (EPE'16 ECCE Europe): 5-9 Sept. 2016*, Karlsruhe, 2016, pp. 1–7.

[27] A. Bardalai *et al.,* "The Influence of Strands and Bundle-Level Arrangements of Magnet Wires on AC Losses in the Winding of High — Speed Traction Machine," in *ICEMS 2018: 2018 21th International Conference on Electrical Machines and Systems (ICEMS) : October 7, Sun.-10, Wed., 2018, Ramada Plaza Jeju Hotel, Jeju, Korea*, Jeju, 2018, pp. 65–69.

[28] R. Wrobel, A. Mlot, and P. H. Mellor, "Contribution of End-Winding Proximity Losses to Temperature Variation in Electromagnetic Devices," *IEEE Trans. Ind. Electron.*, vol. 59, no. 2, pp. 848–857, 2012.